




Magnetofluorescent Nanoprobe for Multimodal and Multicolor Bioimaging

Aditya Yadav, M.Sc¹, Chethana Rao, M.Sc¹, Navneet Chandra Verma, PhD¹, Pushendra Mani Mishra, M.Tech^{1,2}, and Chayan Kanti Nandi, PhD^{1,2,3} 

Abstract

Although, superparamagnetic iron oxide nanoparticles (SPIONs) have extensively been used as a contrasting agent for magnetic resonance imaging (MRI), the lack of intrinsic fluorescence restricted their application as a multimodal probe, especially in combination with light microscopy. In Addition, the bigger size of the particle renders them incompetent for bioimaging of small organelles. Herein, we report, not only the synthesis of ultrasmall carbon containing magneto-fluorescent SPIONs with size ~5 nm, but also demonstrate its capability as a multicolor imaging probe. Using MCF-7 and HeLa cell lines, we show that the SPIONs can provide high contrast mulicolor images of the cytoplasm from blue to red region. Further, single particle level photon count data revealed that the SPIONs could efficaciously be utilized in localization based super resolution microscopy in future.

Keywords

fluorescent iron oxide nanoparticles, multicolor emission, light microscopy, multimodal bioimaging, single particle photon count

Introduction

Over the past few years, superparamagnetic iron oxide nanoparticles (SPIONs), due to their strong magnetic properties and magnetic susceptibility, have been extensively used in magnetic resonance imaging (MRI),¹⁻³ terabit magnetic storage devices,⁴ magnetically guided cancer diagnosis,⁵ theranostic,^{6,7} drug delivery,⁸⁻¹⁰ hyperthermia,¹¹ photoacoustics¹² and cell separation.¹³ Despite such vast applications utilizing their paramagnetic behavior, the exploration of SPIONs as a multimodal probe for various techniques, especially in combination with optical microscopy for high resolution bioimaging is rarely reported. This is attributed to the lack of inherent fluorescence in SPIONs. Henceforth, engineering SPIONs by decorating the fluorescence properties and to get magneto-fluorescent SPIONs is highly desirable to function as a multimodal probe. The magneto-fluorescent behavior of SPIONs will be extremely beneficial as the drawback of 1 technique could easily be rectified by others, e.g. deep tissue cellular imaging, which is not possible in optical microscopy can be achieved by MRI. On the other hand, optical bioimaging is capable of attaining a high spatial resolution which is not possible by MRI imaging.

Nevertheless, few reports on the magneto-fluorescent SPIONs are available in the literature. The common synthesis approach includes the co-assembly of 2 types of nanocrystals having distinct properties into larger colloidal particles at the

mesoscopic scale or by surface functionalization of the SPIONs with fluorescent materials such as quantum dots (QDs) or organic dyes.^{14,15} Strategies involving the template based heterostructure crystal growth have also been reported.^{16,17} However, the conjugated magneto-fluorescent SPIONs, synthesized by the above methods, have a few limitations. For example, the attached fluorescent molecules may suffer quenching in their fluorescence when attached to the nanoparticles and hence compromise with the effective fluorescence quantum yield (QY) and therefore restrict the long term bioimaging. In addition, the tedious multistep synthesis processes are challenging in terms of reproducibility and colloidal stability.

On the other hand, the synthesized magneto-fluorescent, reported so far are majorly very large in size, which obstructs

¹ School of Basic Sciences, Indian Institute of Technology Mandi, Himachal Pradesh, India

² BioX Centre, Indian Institute of Technology, Mandi, Himachal Pradesh, India

³ Advanced Materials Research Centre, Indian Institute of Technology Mandi, Himachal Pradesh, India

Submitted: 06/07/2020. Revised: 05/10/2020. Accepted: 06/10/2020.

Corresponding Author:

Chayan Kanti Nandi, Advanced Materials Research Centre, Indian Institute of Technology Mandi, 175075, Himachal Pradesh, India.

Email: chayan@iitmandi.ac.in



their utilization in viewing smaller organelles inside the cells.¹⁸ The size was found to be a critical criterion that decides the resolving power of the optical bioimaging, the internalization mechanism and kinetics of the cellular uptake efficiency of the nanomaterials into the cell. Moreover, the renal clearance of these bigger size particles is also an issue.¹⁹ Few reports have discussed the small size fluorescent SPIONs. Riju et al. described the synthesis of fluorescein labeled small iron oxide nanoparticles as a T_1 MRI contrasting agent and as a viable tool for cell labeling.²⁰ Jing et al. reported ultrasmall superparamagnetic iron oxide nanoparticles bound with NIR dyes as a theranostic agent.²¹ Jabadurai et al. developed flavin mononucleotide coated fluorescent iron oxide nanoparticles.²² Unfortunately, multistep tedious processes were involved in all these reports, where the fluorescent molecules were conjugated to the SPIONs. While synthesizing small size SPIONs is a challenge in itself, incorporating fluorescence properties adds another hurdle in the process to achieve homogeneous particles without losing both the magnetic and optical properties. Here, we were not only successful in synthesizing ultrasmall magneto-fluorescent carbon composite SPIONs with greater ease via a single step 1 pot procedure but also it demonstrated as a magneto-fluorescent probe for multi-colour bioimaging from blue to red region. Using 2 different cell lines (MCF-7 and HeLa cell lines), we reveal the fast cell internalization of the SPIONs with bright multicolor confocal image of the cytoplasm. Additionally, the fluorescence properties at single particle level have also been studied. These studies reveal that the developed material can be efficiently used as a probe for super resolution microscopy in future.

Materials and Methods

All glasswares were washed with aqua regia, followed by rinsing several times with double distilled water. Ferrocene, Oleic acid, Hexadecene and H_2O_2 were purchased from Merck Chemicals. All chemicals were used without further purification. Double-distilled (18.3 m Ω) deionized water (ELGA PURELAB Ultra) was used throughout the entire process.

The particle morphology was observed by transmission electron microscopy (TEM) using FEI Tecnai TEM equipped with a LaB6 source operating at 200 kV. Powder X-ray diffraction (PXRD) pattern was recorded on a Rigaku Smart Lab diffractometer, using $CuK\alpha$ radiation from 5° to 80° with a scanning rate of 2°/min. Fourier transformed infrared (FTIR) spectra were recorded with Agilent Technologies Cary 6000 series FTIR spectrometer at wavenumber from 400 to 4000 cm^{-1} . X-ray photoelectron spectroscopy (XPS) measurements were carried out on a NEXSA surface analysis model by Thermo Fisher Scientific using $Al-K\alpha$ (1486.6 eV) X-ray radiation. Energy dispersive X-ray analysis (EDX) and elemental analysis of SPIONs was characterized by using a field emission scanning electron microscope (FESEM) FEI Nova SEM-450. The XPS data were acquired with a spot size 400 μm having a standard lens mode. Magnetic properties were analyzed through vibrating sample magnetometer-superconducting

quantum interference device (VSM-SQUID) under the vibrating magnetic field of 4 T at 300 K. UV-Vis absorption spectra were measured with Shimadzu U-2450 UV-Vis spectrophotometer from wavelength range of 200-800 nm. Fluorescence spectra and absolute quantum yield were recorded on the Horiba spectrophotometer.

Confocal Imaging of Cells Labeled With SPIONs

Coverslip Preparation

The glass slides and coverslips were cleaned by incubating in freshly prepared Piranha solution for 30 min and finally washing by MilliQ water in bath sonication then dried under nitrogen.

Cell Culture, Fixation and Staining

Cells were grown in Dulbecco's Modified Eagle Medium (DMEM) with 10% fetal bovine serum. The cells were grown in 6-well plate on the coverslips with a density of 10^4 cells per 100 μl . Each well was filled with 2 ml of cell suspension in growth medium and the cells were allowed to grow overnight for the proper adherence and growth. The growth and the attachment of the cells to the coverslips were examined by an optical microscope. Once the cells reached proper attachment and growth stage, they were stained with SPIONs for 4 h to achieve enough labeling density for confocal microscopy. Finally, the cells were fixed by incubating with 4% paraformaldehyde solution in 1x PBS buffer for 15 min. The fixed cells were then washed 4-6 times by PBS buffer to remove extra agents. The coverslips were fixed on a glass slide before imaging.

Confocal Microscopy

Nikon Eclipse Ti inverted microscope was used for the confocal microscopy and images were acquired using Nikon Nis-Element software. The cell samples were excited by the 4 lasers 401, 488, 561 and 639 nm. Finally, the images were collected by choosing a proper filter set.

Single Molecule Time Trace and Photon Counts

SPIONs were spin coated on a clean glass slide to collect single molecule time traces. The diffraction limited spots produced due to single molecule blinking were observed using 100x Nikon TIRF objective. A 532 nm diode laser with 50 mW maximum power was used. An oil immersion Nikon TIRF objective (100x magnification and 1.49 NA) was mounted on a custom build inverted optical microscope. A 532 nm high pass Dichroic (AHF Analysentechnik) was used to separate the excitation and emission light. Andor EMCCD

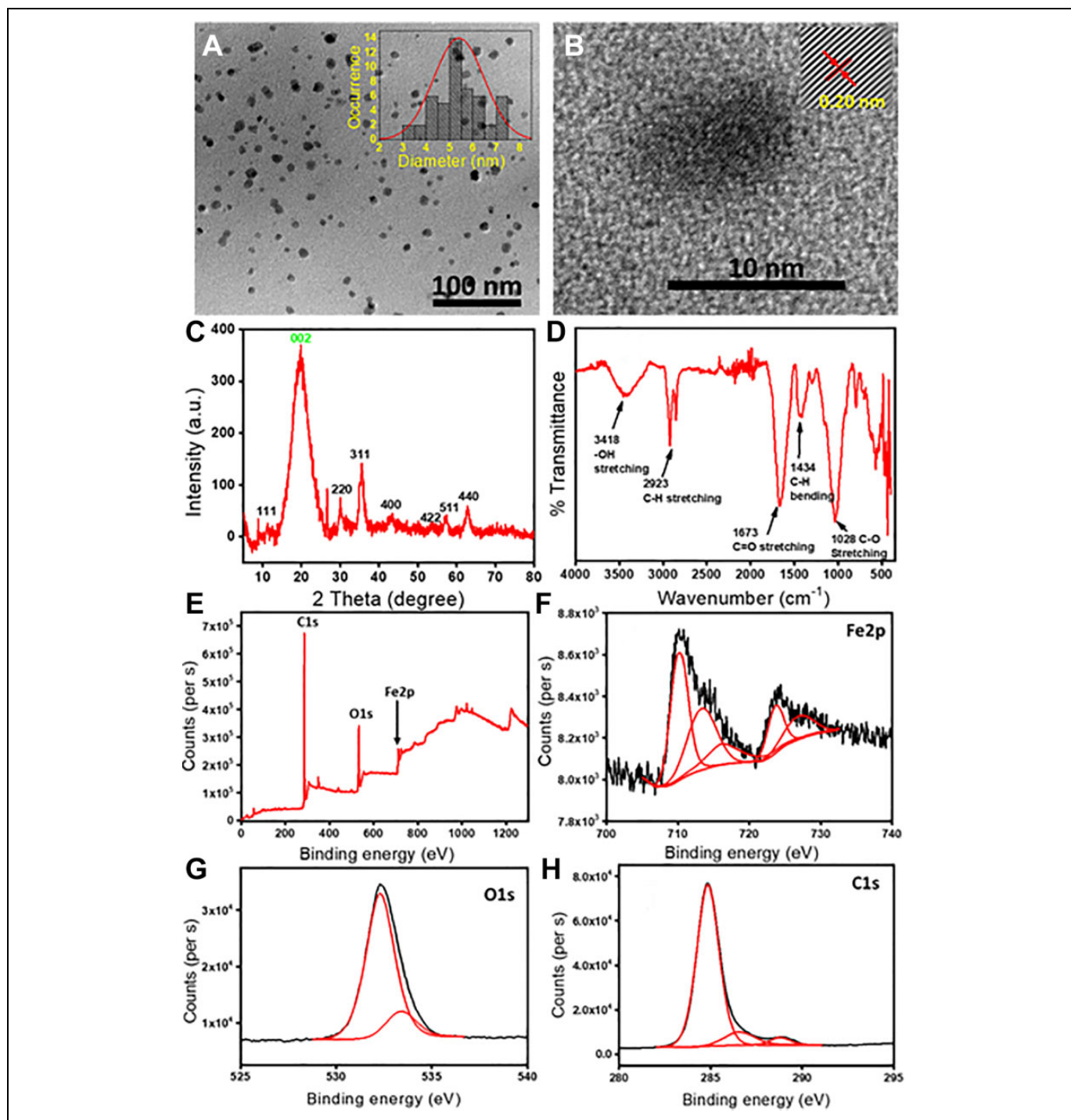


Figure 1. (A) TEM and (B) HRTEM image of SPIONs, (C) PXRD spectra showing the diffraction planes (111), (220), (311), (400), (422), (511), and (440) observed for Fe_3O_4 and (002) plane for graphitic carbon, (D) fourier-transform infrared (FTIR) spectra shows absorption peak for different functional groups, (E) full survey XPS spectra depicting the presence of C1s, O1s and Fe2p, respectively in scan profile, (F) high resolution deconvoluted Fe2p XPS spectra, (G) high resolution deconvoluted O1s XPS spectra and (H) high resolution deconvoluted C1s XPS spectra of SPIONs.

iXon Ultra was used to record the single molecule photon events at the frame rate of 17 MHz and exposure time of 50 ms. The time trajectories were recorded and analyzed using the Andor Solis Software. The incident photons were converted to electrons and subsequent to digital counts by the EMCCD.

The Andor Solis and Matlab were used to extract the total photon counts. The movies recorded under the kinetic mode of EMCCD, time/frame trajectories of the counts/intensity at a given pixel, were obtained for the provided exposure time. These time trajectories were saved for further analysis.

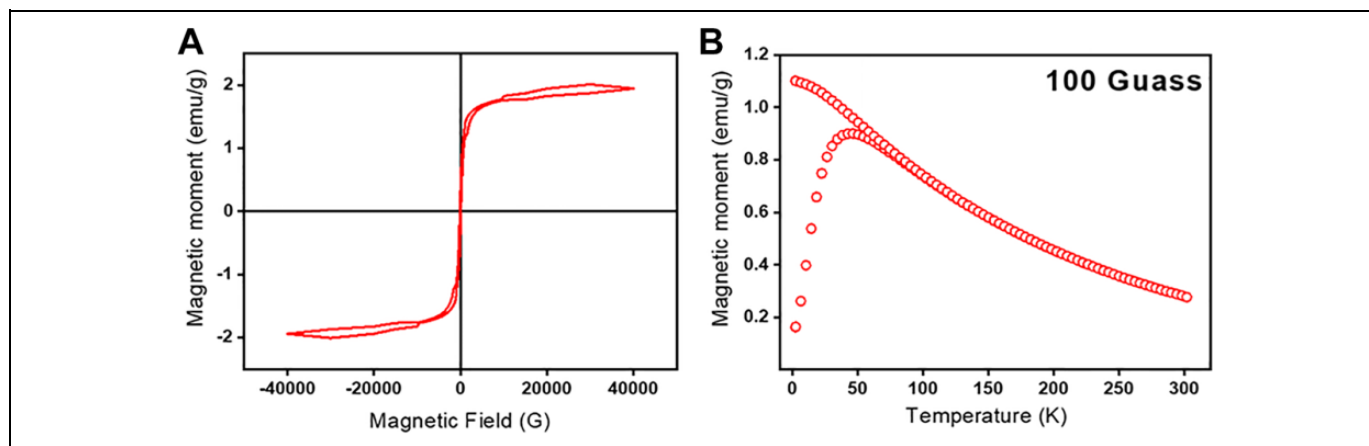


Figure 2. (A) M–H hysteresis curve for SPIONs recorded at room temperature and (B) temperature dependent ZFC and FC curves of SPIONs under a magnetic field of 100 Gauss.

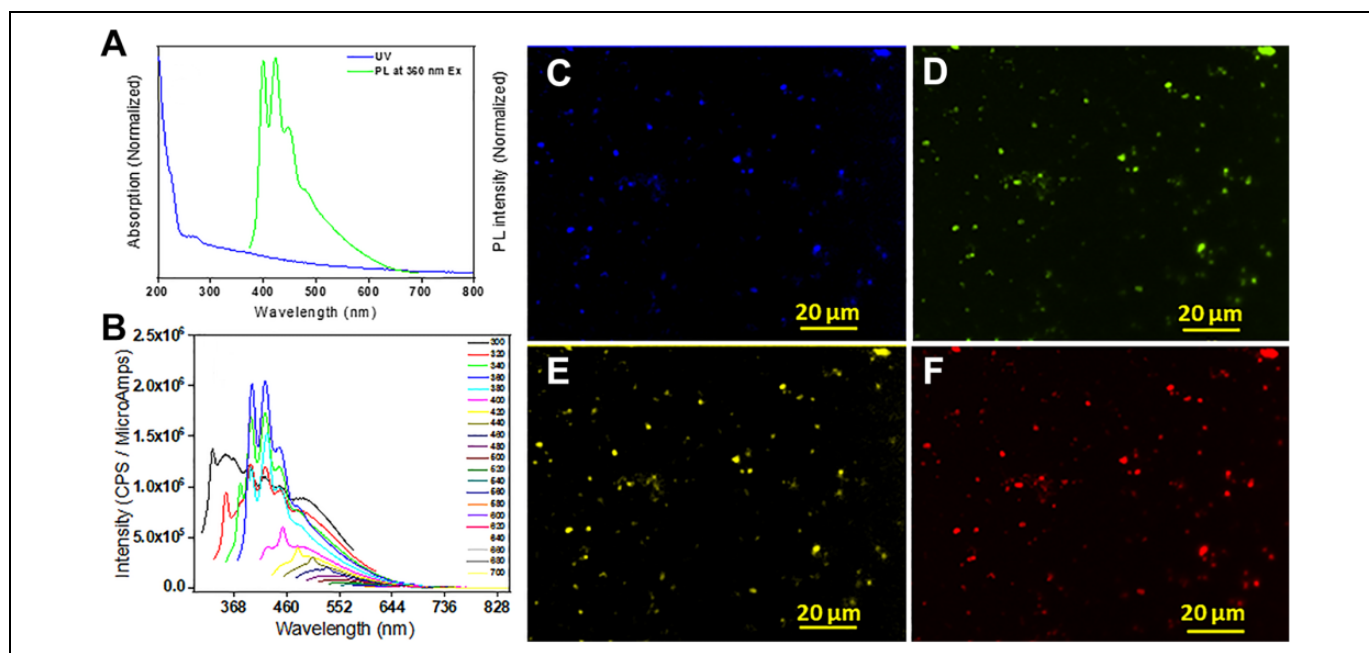


Figure 3. (A) The absorbance (blue) and PL (green) spectra of SPIONs, (B) emission spectra of SPIONs at different excitation wavelengths ranging from 280-700 nm, and (C-F) confocal microscopy images of SPIONs spin coated on glass coverslip showing multicolor emission under different excitation laser wavelengths 401 (blue), 488 (green), 561 (yellow), and 639 (red) nm, respectively.

Result and Discussion

The carbon composite SPIONs were synthesized following the thermal decomposition method. In brief, 0.49 g Ferrocene, 2 ml oleic acid and 20 ml hexadecene were taken in a 3 neck round bottom flask and stirred for 5 min at 25°C under vacuum, to thoroughly mix all the components. Then, the temperature of the mixture was increased to 270°C and the mixture was stirred for 1 h after which it was again cooled to room temperature. Thereafter, 10 ml H₂O₂ (30% w/w) was added to the mixture and the temperature was slowly increased to 130°C and stirred for 1 h. The entire solution was finally cooled down to room temperature. The precipitates from the reaction mixture were

extracted in ethanol solution and centrifuged at 1400 rpm. In order to remove any remaining oleic acid and hexadecene the precipitates were washed with hexane and thereafter the magnetic particles were separated with the help of magnet. Finally, the particles were dried in hot air oven at 80°C and dried powder was collected for various characterizations.

Transmission electron microscopy (TEM) images revealed the formation of homogeneous particles. Further, it also depicted a nearly spherical morphology SPIONs (Figure 1A) with an average size of ~5 nm in diameter. The size was obtained by calculating the average distribution of approximately 50 particles as shown in (Figure 1A, inset). A 2D lattice fringes from high resolution (HR-TEM) image (Figure 1B,

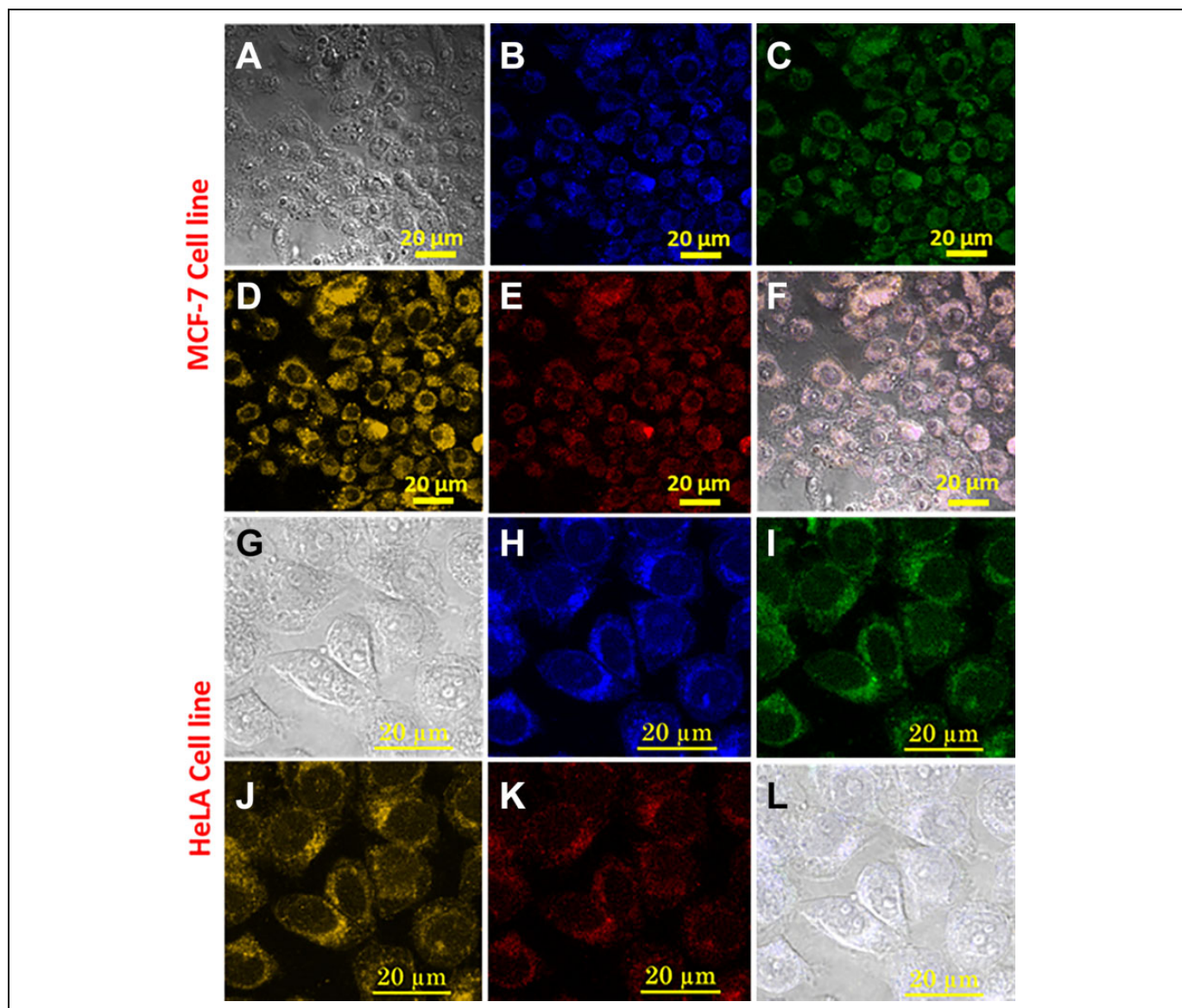


Figure 4. (A) TD image, (B-E) confocal microscopy image of MCF-7 cell line stained with SPIONs under different excitation laser wavelengths 401, 488, 561, and 639 nm, respectively, (F) overlay of Figure 4 (B-E), (G) TD image, (H-K) confocal microscopy image of HeLa cell line stained with SPIONs under different excitation laser wavelengths 401, 488, 561, and 639 nm, respectively and (L) overlay of Figure 4 (H-K).

inset) ~ 0.20 nm confirms the existence of (102) lattice plane of graphitic (sp^2) carbon.^{23,24} Powder X-ray diffraction (PXRD) analysis was performed which further verified the composition of material as an iron carbon composite. The diffraction pattern showed sharp reflections at the 2θ value for magnetite phase of iron. Peaks corresponding to (111), (220), (311), (400), (422), (511), and (440) plane belong to Fe_3O_4 with inverse spinel structure.²⁵ A diffraction peak around 24° represents the (002) plane of graphitic carbon²⁶ thereby validating the presence of graphitized carbogenic nature to the SPIONs (Figure 1D).²⁷

X-ray photoelectron spectroscopy (XPS), a surface sensitive technique also corroborated the presence of magnetite phase of iron. Full survey scan spectra showed the presence of carbon,

oxygen and iron (Figure 1E). Deconvolution of the Fe2p spectrum (Figure 1F) exhibited 2 peaks for Fe $2p_{3/2}$ and 1 peak for $2p_{1/2}$ at binding energy values of 710, 713.5 and 723 eV respectively, corresponding to the inverse spinel structure of Fe_3O_4 , in which both the oxidation states of iron i.e. Fe^{2+} and Fe^{3+} were present. Fe^{2+} occupies the octahedral void while Fe^{3+} occupies both octahedral and tetrahedral voids in a cubic crystal structure. The deconvoluted oxygen O1 s spectrum with peaks at 532 and 533 eV corresponds to C=O and C-O respectively (Figure 1G). Further, the deconvolution of C1 s showed 3 peaks at 284, 286 and 288.7 corresponding to C=C, C-O and -COO functional groups, respectively (Figure 1H).²⁸ The elemental composition obtained from the energy dispersive X-ray analysis (EDX) further confirmed the presence of C, O and Fe

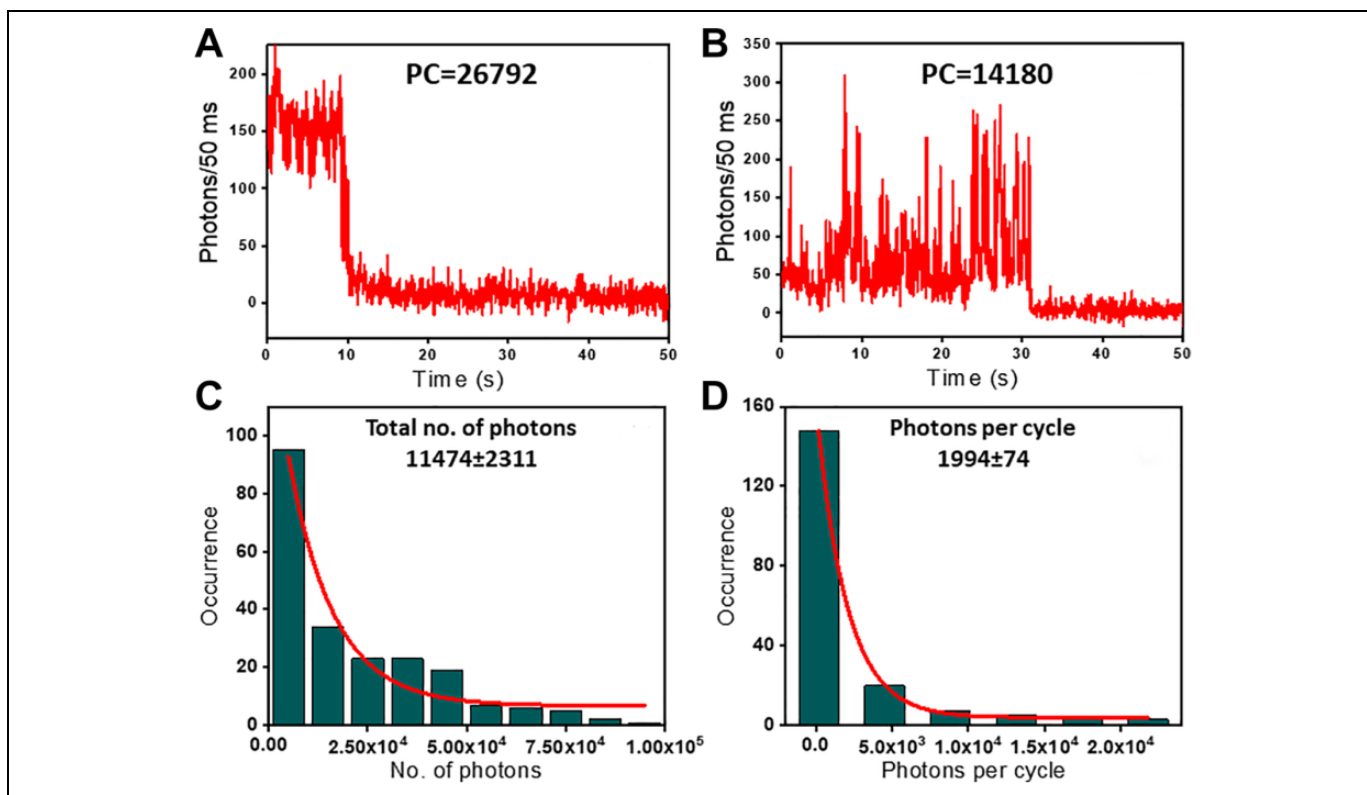


Figure 5. (A, B) Single molecule fluorescence time traces of SPIONs, both single step photobleaching and blinking were observed, (C) total numbers of photos found were 11474 and (D) photons per cycle were found to be 1994.

(Figure S1). The Fourier-transform infrared (FTIR) spectroscopic measurements were also carried out to get to know about the functional groups in carbon coated SPIONs. The peaks observed at 1434 cm^{-1} and 2923 cm^{-1} are due to C-H bending and stretching vibrations respectively. Further, a peak at 1028 cm^{-1} belongs to C-O stretching and at 1673 cm^{-1} to C=O stretching. O-H stretching frequency was noted at 3418 cm^{-1} (Figure 1D).

VSM (vibrating sample magnetometer) measurement was carried out to find out the magnetic properties of the material. A material is said to be superparamagnetic if it magnetized up to its saturation magnetization during the application of external magnetic field and on removal of magnetic field it should not exhibit any residual magnetic interaction.²⁹ A magnetic hysteresis (M-H) curve (Figure 2A) shows saturation magnetization (Ms) at 1.94 emu/g , which seems to be in the little lower range. This could be attributed to the ultrasmall size of the SPIONs, which might show the canting effect.³⁰ It was previously shown that on decreasing the size of magnetic core the magnetic saturation value decreases.³¹ Moreover, once the applied magnetic field was removed, the magnetic particles did not retain any residual magnetism at room temperature. Fe_3O_4 crystals with diameters of 20 nm or less are superparamagnetic as there is no hysteresis after applying an external magnetic field because each crystal acts as a single magnetic domain.³² Remanent magnetization (M_r) 0.35 emu/g , is very low which further verified superparamagnetic behavior. Little broadening

in M-H hysteresis loop reveals a weak ferromagnetic nature of SPIONs at room temperature as coercivity (H_c) comes to be 134 .^{33,34} Temperature dependent zero field cooled (ZFC) and field cooled (FC) also suggest about the superparamagnetic nature, to achieve the superparamagnetic nature blocking temperature (T_B) should be much lower than room temperature.³⁵ ZFC and FC in (Figure 2B) therefore confirmed the superparamagnetic behavior of material as T_B was found to be $\sim 50\text{ K}$. Also, the T_B value is related to the particle volume (V) and effective anisotropy (K_{eff}) by the following equation; $V = 25k_B T_B / K_{\text{eff}}$, where k_B is the Boltzmann constant.³⁶ According to this, lower the T_B value lower will be the volume, $T_B \sim 50\text{ K}$ again confirms the smaller size of the material. The shape of the ZFC and FC curves were indicative of the smaller particle size and narrower size distribution for SPIONs³⁷ which is in accordance with TEM data. Hence, it could be concluded that the material has enough magnetic properties to be used as MRI contrasting agent.

Next, we measured the optical properties of the magneto fluorescent SPIONs. A broad absorption spectrum ranging from 200 to 800 nm was observed. This could be attributed due to the carbon dots like behavior of carbon coated on SPIONs (Figure 3A).³⁸ The observed emission spectra also support the typical signature of carbogenic nanomaterials. A broad emission spectrum with an emission maximum at 423 nm under 360 nm excitation was observed (Figure 3A). Further, the carbon coated SPIONs shows the excitation

dependent multicolor emission (Figure 3B) as normally obtained in carbon dots.³⁹ The observed emission properties of SPIONs may be attributed to surface energy traps emission from rich carboxyl and hydroxyl groups, as reported earlier for carbonogenic nanomaterials. The multicolor emission was also observed on the spin coated drop dried sample when observed in a confocal microscope using different laser excitation systems, along with proper optical filters. The sample was excited with 4 different lasers 401, 488, 532, and 639 nm and the different color emission (blue, green, yellow and red respectively) are presented in Figure 3C-F. The data clearly show that the SPIONs could be used as a multicolor imaging probe in real cellular systems.

The above results motivated us to examine the bioimaging of SPIONs in 2 different cancer cell line i.e. MCF-7 and HeLa cells. The cells were grown in Dulbecco's Modified Eagle Medium (DMEM) with 10% fetal bovine serum and further seeded on a glass coverslip with density of 10^4 cells per 100 μ l. Once the cells were properly adhered, they were incubated with SPIONs for 4 h in order to achieve enough labeling density for imaging in confocal microscope. The cells were then washed with PBS buffer several times to remove any unbound SPIONs. Finally, the stained cell lines were examined through the confocal microscope. Surprisingly, Figure 4 shows that the SPIONs have the capability to show the multicolor bioimaging with greater efficiency, but with a little decrease in intensity in the red region in both the cell lines. This could be justified by the emission intensity of the bulk measurement. It could be seen in Figure 3B that the emission intensity is maximum in the blue and green region, while it decreases substantially in the red region. As a result, in the confocal image, the number of excited particles is also less and hence the emission intensity decreases in the cells.

Finally, the fluorescence emission behavior of SPIONs was performed at the single particle level. The dispersed spincoated particles on a coverslip were illuminated by a 532 nm laser and corresponding fluorescence was collected by set of appropriate dichroics and filters. (Figure 5A and B) show both single step and multistep bleaching of the single SPIONs. Interestingly, 60% of the observed time traces showed a single step bleaching whereas 40% of the particles showed the fluorescence intermittency which is a general phenomenon of the carbon based fluorescence materials.⁴⁰ In addition, the particles show total photocounts as high as $\sim 12,000$ (Figure 5C and D), which is much higher than some earlier reported organic dyes and fluorescent proteins (Table S1).⁴¹ In addition, we also calculated the absolute quantum yield (QY) using integrated sphere method and the QY was found to be $\sim 1\%$. So, we hope that, the newly synthesized magneto-fluorescent SPIONs have a bright future as a fluorescent probe in single molecule localization-based super resolution microscopies techniques.

Conclusion

In summary, we have successfully synthesized carbon coated magneto-fluorescent ultrasmall superparamagnetic iron oxide nanoparticles with a size ~ 5 nm, with a greater ease in a single

step 1 pot method. Along with their magnetic properties, the SPIONs have the capability to be used as a multicolor imaging probe. Using MCF-7 and HeLa cell lines, we have shown that the SPIONs efficiently stained the cytoplasm of the cells. Further, single particle level photon count study reveals that the SPIONs could efficiently be used in localization based super resolution microscopy in future.

Author Contributions

A.Y. designed all the experiments. C.R. performed the TEM measurement. N.C.V. helped in analyzing the optical data at single particle level. P.M.M. completed the cell culture experiments. C.K.N guided the complete project and wrote the manuscript with the help of A.Y.

Acknowledgments

We are thankful Advanced Material Research Centre (AMRC) and BioX center of IIT Mandi, India for providing the facilities and the sophisticated instruments. A.Y. thanks to the Council of Scientific and Industrial Research (CSIR JRF:09/1058(0014)/2019-EMR-I), N.C.V. thanks the Council of Scientific and Industrial Research (CSIR SRF:9/1058(07)/2017-EMR-I), P.M.M. thanks the Council of Scientific and Industrial Research (CSIR JRF:09/1058(0013)/2019-EMR-I) and C.K.N. acknowledges IIT Mandi for the financial support.


Declaration of Conflicting Interests

The author(s) declared no potential conflicts of interest with respect to the research, authorship, and/or publication of this article.

Funding

The author(s) received no financial support for the research, authorship, and/or publication of this article.

ORCID iD

Chayan Kanti Nandi  <https://orcid.org/0000-0002-4584-0738>

Supplemental Material

Supplemental material for this article is available online.

References

1. Brähler M, Georgieva R, Buske N, et al. Magnetite-loaded carrier erythrocytes as contrast agents for magnetic resonance imaging. *Nano Lett.* 2006;6(11):2505–2509.
2. Yan L, Amirshaghghi A, Huang D, et al. Protoporphyrin IX (PpIX)-coated superparamagnetic iron oxide nanoparticle (SPION) nanoclusters for magnetic resonance imaging and photodynamic therapy. *Adv Funct Mater.* 2018;28(16):1707030.
3. Qin J, Laurent S, Jo YS, et al. A high-performance magnetic resonance imaging T2 contrast agent. *Adv Mater.* 2007;19(14):1874–1878.
4. O'handley RC. *Modern Magnetic Materials: Principles and Applications.* Wiley; 2000.
5. Sabnis S, Sabnis NA, Raut S, Lacko AG. Superparamagnetic reconstituted high-density lipoprotein nanocarriers for magnetically guided drug delivery. *Int J Nanomed.* 2017;12:1453–1464.
6. Santhosh PB, Ulrich NP. Multifunctional superparamagnetic iron oxide nanoparticles: promising tools in cancer theranostics. *Cancer Lett.* 2013;336(1):8–17.

7. Dadfar SM, Roemhild K, Drude NI, et al. Iron oxide nanoparticles: diagnostic, therapeutic and theranostic applications. *Adv Drug Deliv Rev.* 2019;138:302–325.
8. Torchilin VP. Multifunctional, stimuli-sensitive nanoparticulate systems for drug delivery. *Nat Rev Drug Discov.* 2014;13(11):813–827.
9. Zhuang M, Du D, Pu L, et al. SPION-decorated exosome delivered BAY55-9837 targeting the pancreas through magnetism to improve the blood GLC response. *Small.* 2019;15(52):1903135.
10. Miranda MS, Miranda MS, Domingues RMA, et al. Development of inhalable superparamagnetic iron oxide nanoparticles (spions) in microparticulate system for antituberculosis drug delivery. *Adv Healthc Mater.* 2018;7(15):1800124.
11. Hayashi K, Nakamura M, Sakamoto W, et al. Superparamagnetic nanoparticle clusters for cancer theranostics combining magnetic resonance imaging and hyperthermia treatment. *Theranostics.* 2013;3(6):366.
12. Grootendorst DJ, Jose J, Fratila RM, et al. Evaluation of superparamagnetic iron oxide nanoparticles (Endorem[®]) as a photoacoustic contrast agent for intra-operative nodal staging. *Contrast Media Mol Imaging.* 2013;8(11):83–91.
13. Clement JH, Schwalbe M, Buske N, et al. Differential interaction of magnetic nanoparticles with tumor cells and peripheral blood cells. *J Cancer Res Clin Oncol.* 2006;132(5):287–292.
14. Chen O, Riedemann L, Etoc F, et al. Magneto-fluorescent core-shell supernanoparticles. *Nat Commun.* 2014;5:1–8.
15. Pahari SK, Olszakier S, Kahn I, Amirav L. Magneto-fluorescent yolk-shell nanoparticles. *Chem Mater.* 2018;30(3):775–780.
16. Ge J, Hu Y, Zhang T, Yin Y. Superparamagnetic composite colloids with anisotropic structures. *J Am Chem Soc.* 2007;129(29):8974–8975.
17. Li K, Liu B. Polymer-encapsulated organic nanoparticles for fluorescence and photoacoustic imaging. *Chem Soc Rev.* 2014;43(18):6570–6597.
18. Tiwari A, Kumar R, Shefi O, Randhawa JK. Fluorescent mantle carbon coated core-shell SPIONS for neuroengineering applications. *ACS Appl Bio Mater.* 2020;3(7):4665–4673.
19. Chen YS, Hung YC, Liao I, Huang GS. Assessment of the in vivo toxicity of gold nanoparticles. *Nanoscale Res Lett.* 2009;4:858.
20. Bhavesh R, Lechuga-Vieco AV, Ruiz-Cabello J, Herranz F. T1-MRI fluorescent iron oxide nanoparticles by microwave assisted synthesis. *Nanomaterials.* 2015;5(4):1880–1890.
21. Cai J, Dao P, Chen H, et al. Ultrasmall superparamagnetic iron oxide nanoparticles-bound NIR dyes: novel theranostic agents for Alzheimer's disease. *Dye Pigment.* 2020;173:107968.
22. Jayapaul J, Hodenius M, Arns S, et al. FMN-coated fluorescent iron oxide nanoparticles for RCP-mediated targeting and labeling of metabolically active cancer and endothelial cells. *Biomaterials.* 2011;32(25):5863–5871.
23. Wang H, Shen J, Li Y, et al. Magnetic iron oxide-fluorescent carbon dots integrated nanoparticles for dual-modal imaging, near-infrared light-responsive drug carrier and photothermal therapy. *Biomater Sci.* 2014;2(6):915–923.
24. Tian L, Ghosh D, Chen W, Pradhan S, Chang X, Chen S. Nanosized carbon particles from natural gas soot. *Chem Mater.* 2009;21(13):2803–2809.
25. Wang X, Liu Y, Arandiyani H, et al. Uniform Fe₃O₄ microflowers hierarchical structures assembled with porous nanoplates as superior anode materials for lithium-ion batteries. *Appl Surf Sci.* 2016;389:240–246.
26. Verma NC, Yadav A, Nandi CK. Paving the path to the future of carbogenic nanodots. *Nat Commun.* 2019;10(1):2391.
27. Oliveira LC, Rios RV, Fabris JD, Garg V, Sapag K, Lago RM. Activated carbon/iron oxide magnetic composites for the adsorption of contaminants in water. *Carbon N Y.* 2002;40(12):2177–2183.
28. Tiwari A, Verma NC, Singh A, Nandi CK, Randhawa JK. Carbon coated core-shell multifunctional fluorescent SPIONS. *Nanoscale.* 2018;10(22):10389–10394.
29. Wahajuddin SA. Superparamagnetic iron oxide nanoparticles: magnetic nanoplateforms as drug carriers. *Int J Nanomed.* 2012;7:3445.
30. Krycka KL, Borchers JA, Booth RA, et al. Origin of surface canting within Fe₃O₄ nanoparticles. *Phys Rev Lett.* 2014;113:147203.
31. Kim BH, Lee N, Kim H, et al. Large-scale synthesis of uniform and extremely small-sized iron oxide nanoparticles for high-resolution T1 magnetic resonance imaging contrast agents. *J Am Chem Soc.* 2011;133(32):12624–12631.
32. Dulińska-Litewka J, Łazarczyk A, Hałubiec P, Szafranski O, Karnas K, Karewicz A. Superparamagnetic iron oxide nanoparticles-current and prospective medical applications. *Materials (Basel).* 2019;12(4):617.
33. Marolt M, Jaglicic Z. *Superparamagnetic materials.* Semin Messtrado, Univ; 2014.
34. Sung HWF, Rudowicz C. A closer look at the hysteresis loop for ferromagnets - A survey of misconceptions and misinterpretations in textbooks. *arXiv Prepr. cond-mat/0210657*; 2002.
35. Rumpf K, Granitzer P, Morales PM, Poelt P, Reissner M. Variable blocking temperature of a porous silicon/Fe₃O₄ composite due to different interactions of the magnetic nanoparticles. *Nanoscale Res Lett.* 2012;7:445.
36. Knobel M, Nunes WC, Socolovsky LM, De Biasi E, Vargas JM, Denardin JC. Superparamagnetism and other magnetic features in granular materials: a review on ideal and real systems. *J Nanosci Nanotechnol.* 2008;8(6):2836–2857.
37. Pereira GF, Costa FN, Souza JA, Haddad PS, Ferreira FF. Parametric rietveld refinement and magnetic characterization of superparamagnetic iron oxide nanoparticles. *J Magn Magn Mater.* 2018;456:108–117.
38. Sun YP, Zhou B, Lin Y, et al. Quantum-sized carbon dots for bright and colorful photoluminescence. *J Am Chem Soc.* 2006;128(24):7756–7757.
39. Sharma A, Gadly T, Gupta A, Ballal A, Ghosh SK, Kumbhakar M. Origin of excitation dependent fluorescence in carbon nanodots. *J Phys Chem Lett.* 2016;7(18):3695–3702.
40. Verma NC, Rao C, Singh A, Garg N, Nandi CK. Dual responsive specifically labelled carbogenic fluorescent nanodots for super resolution and electron microscopy. *Nanoscale.* 2019;11(14):6561–6565.
41. Verma NC, Rao C, Nandi CK. Nitrogen-doped biocompatible carbon dot as a fluorescent probe for STORM nanoscopy. *J Phys Chem C.* 2018;122(8):4704–4709.